Increasing PV Hosting Capacity with an Adjustable Hybrid Power Flow Model

Luomeng Zhang, *Student Member, IEEE,* Hongxing Ye, *Senior Member, IEEE,* Fei Ding, *Senior Member, IEEE,* Zuyi Li, *Senior Member, IEEE,* Mohammad Shahidehpour, *Fellow, IEEE*

***Abstract*—Physical constraints must be enforced when distributed energy resources, such as PV, are integrated into distribution network. Hosting capacity (HC) is thus introduced to define the maximum renewable generation that distribution system can accommodate. When the grid is further pushed towards decarbonization, improving HC becomes even more important. This work presents a hybrid adjustable power flow model to increase the uncertainty-proof HC, aiming to securely and cost-effectively utilize flexible resources. We propose a novel hybrid relaxation approach to convexifying a two-stage AC model with variable uncertainty set. An iterative algorithm is designed to solve the problem. We perform the case study in a single-phase 141-node system and a three-phase 33-bus system. The proposed approach shows promising performance in accuracy, convergence, and robustness.**

***Index Terms*—Uncertainty, Renewable, Surrogate Affine Policy, Convexification**

NOMENCLATURE

A. Sets and Indices

$\mathcal{T}, t$	Set/Index of time periods.
$\mathcal{N}, n$	Set/Index of PVs.
$\mathcal{M}, m$	Set/Index of loads.
$\mathcal{L}, l$	Set/Index of GTGs.
$\mathcal{R}, r$	Set/Index of SVCs.
$\mathcal{I}, i$	Set/Index of nodes.
$\mathcal{B}, (i,j)$	Set/Index of distribution lines.

B. Variables

$P_{n,t}^{pv,s,\phi}, Q_{n,t}^{pv,s,\phi}$	Scheduled active/reactive power of n-th PV at time t.
$P_{l,t}^{g,\phi}, Q_{l,t}^{g,\phi}$	Scheduled active/reactive power of l-th GTG at time t.
$Q_{r,t}^{svc,\phi}$	Scheduled reactive power of r-th SVC at time t.
$C_n^{pv,\phi}$	Capacity of n-th PV.
$C_r^{svc,\phi}$	Capacity of r-th SVC.
$\lambda_r^{svc,\phi}$	Binary variable of r-th SVC, equaling 1 if installed, otherwise 0.
$u_{n,t}^{up,\phi}, u_{n,t}^{down,\phi}$	Upper/Lower bound of OIR of n-th PV at time t.
$u_{m,t}^{up,\phi}, u_{m,t}^{down,\phi}$	Upper/Lower bound of OIR of m-th load at time t.
$W_{i,t}^{\phi}, T_{ij,t}^{\phi}, R_{ij,t}^{\phi}$	Auxiliary variables of SOC relaxation.
$\boldsymbol{\pi}$	Non-negative multiplier.
$\hat{\boldsymbol{F}}^{\boldsymbol{P}}, \hat{\boldsymbol{F}}^{\boldsymbol{Q}}, \hat{\boldsymbol{F}}^{\boldsymbol{z}}$	Surrogate affine policy of active power, reactive power and auxiliary variables.

C. Parameters

$k_{n,t}^{low,\phi}, k_{n,t}^{up,\phi}$	Lower/Upper bound coefficients for the confidence interval of n-th PV at time t.
$k_{n,t}^{f,\phi}$	Forecast expectation coefficient of n-th PV at time t.
$P_{m,t}^{low,\phi}, P_{m,t}^{up,\phi}$	Lower/Upper bound for the confidence interval of m-th load at time t.
$P_{m,t}^{l,f,\phi}$	Forecast expectation of m-th load at time t.
$G_{ij}^{\phi}, B_{ij}^{\phi}$	Conductance/Susceptance components of the admittance matrix.
$\underline{\theta}_n^{pv,\phi}, \overline{\theta}_n^{pv,\phi}$	Lower/Upper limit of power factor angle of n-th PV.
$\alpha_l^{p,\phi}, \alpha_l^{q,\phi}$	Coefficient of minimum active power and maximum phase-lead operation of l-th GTG.
$\theta_l^{g,\phi}$	Power factor of l-th GTG.
$C_l^{g,\phi}$	Capacity of l-th GTG.
$X^{svc,\phi}$	Number of installed SVC.
$\overline{C}_r^{svc,\phi}$	Maximum allowable capacity of r-th SVC.
$\underline{V}^{\phi}, \overline{V}^{\phi}$	Lower/Upper bound of voltage.
N_u	Length of the uncertainty vector.
$\overline{S}_{ij}^{\phi}$	Apparent power capacity of distribution line.
$V_{i,t}^{\phi^{(0)}}, \theta_{i,t}^{\phi^{(0)}}$	Nominal point of voltage magnitude/angle at i-th node at time t.

I. INTRODUCTION

Renewable energy such as photovoltaic (PV) in power systems is regarded as the important contributor to carbon neutrality. With government support and declining per wart cost of PV, worldwide solar energy production has boomed in the past decades. At least 139.4 GW of PV have been installed and commissioned globally in 2020 [1]. At the end of 2020, the total cumulative installed capacity of PV reached 760.4 GW.

However, the rapidly rising penetration of PV has been posing challenges to the distribution network, such as reverse power, over-voltage, and real-time power balance [2]. According to ANSI C84.1-2011 [3], the voltage in distribution system should remain within 5% of its nominal value. The power injection from high PV penetration can easily cause exceeding-security-limit voltage. In the meantime, PV generation is regarded semi-controllable due to its intermittent and random nature, which makes it difficult to balance the power

This work is supported by State Grid under No. 5100-202156006A-0-0-00. (*Corresponding Author: Hongxing Ye*)

L. Zhang and H. Ye are with MOE KLINNS Lab, Xi'an Jiaotong University, Xi'an, China. F. Ding is with U.S. National Renewable Energy Lab, CO 80401, U.S. Z. Li and M. Shahidehpour are with Illinois Institute of Technology, IL 60616, U.S.

in real time. Utilities thus need to determine the maximum PV installation capacity that they can accommodate without violating any operation constraints. The maximum renewable installation capacity is defined as the hosting capacity (HC) [4], [5]. The concept of renewable HC receives well attention in the power community, and some utilities have used HC in their production systems.

The HC literature is categorized into static HC (SHC) [6]–[13] and dynamic HC (DHC) [14]–[16]. SHC is typically viewed as a static parameter determined for PV interconnection, and the DHC considers the dynamic characteristics of power systems. Most literature employ Monte Carlo based methods to determine the HC [6]–[9], [17]. The basic idea is to perform power flow simulations with a large set of randomly generated samples, and then find the worst-case snapshot for any operation constraint violation, such as over/undervoltage, voltage imbalance, conductor thermal limit violation, transformer overload, etc.

In the early literature, HC is attained from passive simulations, where no recourse actions are taken in operation. It is hence regarded conservative as the absence of recourse actions will prevent utilities from accommodating more PV [18]. In recent years, some researches consider the recourse action in determining HC. Among them, reference [10] develops a bi-level model to determine the battery storage system (BSS) allocation for overvoltage mitigation. Active distribution network (ADN) in [11] is managed to maximize HC. In [12], quadratic power control is used to improve the mitigation performance of BSS and increase HC with a non-linear programming model. Reference [19] proposes a reactive power flow control method for PV inverters to provide voltage regulations.

Uncertainty has been taken into consideration recently. The three predominant techniques used to handle uncertainty have been stochastic analysis [4], [20], [21], stochastic optimization [22]–[24] and robust optimization [25]–[27]. These interesting works have made important progress in handling uncertainty for HC. In the stochastic analysis (SA), Monte Carlo simulation is used to generate the random scenarios of uncertainty. The stochastic optimization (SO) often models a number of scenarios of uncertainty by utilizing probability density function (PDF). The worst-case oriented robust optimization (RO) can guarantee the feasibility of decisions by considering the worst-case scenario from the uncertainty intervals. However, finite scenarios condensed from infinite uncertainty in SO or SA may lead to HC overly pessimistic or optimistic. RO often requires efforts in solving the intractable NP-hard problems with max-min structure and variable uncertainty set. Moreover, the explicit recourse action, which denotes the readily determined dispatch strategy of flexible resources when uncertainty is materialized, is absent in the aforementioned works.

On the other hand, it is still challenging to balance the model accuracy and solution quality of the mathematical optimization approach. When AC model is employed, heuristic methods are often used in the solution approaches [11], [22]. However, the solution quality of heuristic methods may not be guaranteed, and extensive computation efforts are often required. In the meantime, when linearized approximation [23]–[27], such as DistFlow model, is used, it may be not accurate enough and lead to HC inaccuracy. Considering uncertainty makes it even more challenging. Both SO and RO approaches could significantly increase the computational complexity. Hence, in most existing work of mathematical optimization approach, either heuristic methods or linearized models are employed to find HC.

Aiming to capture the uncertainty of PV and load while guaranteeing model accuracy and solution quality, this paper proposes an adjustable approach based on a novel hybrid convexification model, which can also provide explicit recourse action for flexible resources. As the proposed model is immune to uncertainty, we name the HC attained as uncertainty-proof HC. Variable uncertainty set of PV generation and load demand is introduced in the model. Surrogate Affine Approximation method proposed in [28] is employed to solve the problem. When uncertainty is materialized, utilities can take pre-optimized actions for controllable resources, such as PV inverters, static var compensators (SVCs) and distributed gas turbine generators (GTGs), to comply with operation constraints. The contributions of this paper are threefold.

- This paper presents an adjustable AC power flow model to increase uncertainty-proof HC. Inspired by robust work, this model gives a solution that is immune to any uncertainty. In the meantime, the model has variable uncertainty set, as HC is to be determined. The HC, location, and size of SVC are decision variables at the first stage, i.e. planning stage, while the uncertainty from PV generation and load demand is accommodated by distributed energy resources (DERs) at the second stage, i.e. operation stage.
- This work proposes a novel hybrid convexification approximation and successive algorithm to find the solution. They balance the model accuracy and solution quality. The second order cone relaxation is employed for power flow model at the first stage, while the second stage integrates the affine policy and an iterative linearization technique. The proposed solution approach iteratively approximates the original AC model. The hybrid approximation and algorithm could have wide applications in two-stage or multi-stage models.
- The approach provides an explicit re-dispatch policy for flexible DERs. The re-dispatch policy is an analogy to the participation coefficient in Automatic Generation Control (AGC), except that it is optimally determined. Flexible resources can be re-dispatched based on a closed-form solution when the uncertainty is materialized. Besides, re-dispatch action is continuous and can be applied in different timescales.

The rest of this paper is organized as follows. In Section II, the adjustable hybrid power flow model is proposed. In Section III, the solution approach is presented. Case studies are given in Section IV. Section V concludes this paper.

II. Problem Formulation

This section presents an adaptive optimization model for the uncertainty-proof HC. The objective is to find the largest

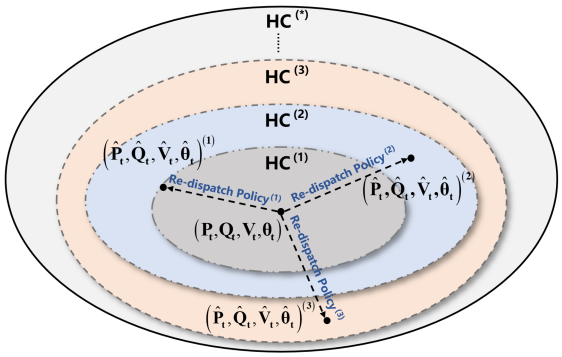

Fig. 1. Diagrammatic sketch of the proposed adaptive framework to increase uncertainty-proof HC. The uncertainty set of PV output varies with HC, and any uncertainty can be safely accommodated based on the re-dispatch policy.

PV capacity that the distribution system can accommodate with flexible resources. The system is guaranteed to mitigate uncertainty when the uncertainty is materialized. Fig.1 illustrates the proposed framework. Let $\boldsymbol{P}_t$, $\boldsymbol{Q}_t$, $\boldsymbol{V}_t$, and $\boldsymbol{\theta}_t$ be the vectors of scheduled active power, reactive power of controllable components, voltage magnitude, and phase angle, respectively. They are optimally determined together with HC of PV, SVC siting and sizing at Stage-1, and they are adjustable to accommodate any uncertainty from PV output and load demand at Stage-2. The PV output uncertainty set is a function of PV installation capacity, and thus is modeled as a decision variable. $\hat{\boldsymbol{P}}_t$, $\hat{\boldsymbol{Q}}_t$, $\hat{\boldsymbol{V}}_t$ and $\hat{\boldsymbol{\theta}}_t$ are new variables at Stage-2 based on the re-dispatch policy. Therefore, the variables at Stage-1 represent planning decisions, while the re-dispatch at Stage-2 represent operation decision. The short-term operation decisions that may change drastically in the real condition are simplified as the re-dispatch variables at Stage-2. As a side note, utility can also perform the simulation in the day-ahead scheduling to get a more accurate short-term re-dispatch policy in the intraday scheduling.

A. Confidence Interval of PV Generation and Load Uncertainty

The deviations from PV forecast output and load forecast are considered as uncertainty. It is noted that the beta distribution function is often used to characterize PV output. We assume the deviations from PV generation and load forecast follow the Gaussian distribution. In the three-phase distribution system, the materialized active power output from PV n and demand from load m of phase ϕ are denoted as

$$P_{n,t}^{pv,\phi} = P_{n,t}^{pv,f,\phi} + \epsilon_{n,t}^{pv,\phi},\ \ \epsilon_{n,t}^{pv,\phi} \sim N\left(0, \sigma_1^2\right), \forall t \in \mathcal{T}, \quad (1)$$

$$P_{m,t}^{l,\phi} = P_{m,t}^{l,f,\phi} + \epsilon_{m,t}^{l,\phi},\ \ \epsilon_{m,t}^{l,\phi} \sim N\left(0, \sigma_2^2\right), \forall t \in \mathcal{T}, \quad (2)$$

where $P_{n,t}^{pv,\phi}$, $P_{n,t}^{pv,f,\phi}$ and $\epsilon_{n,t}^{pv,\phi}$ are materialized PV output, forecast expectation of PV output, and deviation from PV forecast at time t, respectively. $P_{m,t}^{l,\phi}$, $P_{m,t}^{l,f,\phi}$ and $\epsilon_{m,t}^{l,\phi}$ denote actual load demand, forecast expectation of load, and deviation from load forecast at time t, respectively. $\mathcal{T}$ stands for the set of time periods. σ_1^2 and σ_2^2 are the variance of uncertainty. PV output is directly proportional to its capacity and solar intensity, and the area is directly proportional to the capacity [29]. Let $C_n^{pv,\phi}$ denote the capacity of n-th PV. Let $\mathcal{N}$ denote the set of PV. Then, the confidence interval of $\epsilon_{n,t}^{pv,\phi}$ can be described as $[-k_{n,t}^{low,\phi}, k_{n,t}^{up,\phi}]C_n^{pv,\phi}$, where $k_{n,t}^{low,\phi}$ and $k_{n,t}^{up,\phi}$ are lower and upper bounds coefficients for the confidence interval. The PV generation confidence interval can be further rewritten as

$$P_{n,t}^{pv,\phi} \in \left[\left(k_{n,t}^{f,\phi} - k_{n,t}^{low,\phi}\right) C_n^{pv,\phi}, \left(k_{n,t}^{f,\phi} + k_{n,t}^{up,\phi}\right) C_n^{pv,\phi}\right], \quad \forall t \in \mathcal{T}, \quad (3)$$

where parameter $k_{n,t}^{f,\phi}$, $k_{n,t}^{low,\phi}$ and $k_{n,t}^{up,\phi}$ can be extracted from historical data. $k_{n,t}^{f,\phi}$ is the forecast expectation of PV per unit. The load demand's expectation and confidence interval are assumed known parameters, and load demand range is described as

$$P_{m,t}^{l,\phi} \in \left[P_{m,t}^{l,f,\phi} - P_{m,t}^{low,\phi}, P_{m,t}^{l,f,\phi} + P_{m,t}^{up,\phi}\right], \forall t \in \mathcal{T}, \quad (4)$$

where $P_{m,t}^{low,\phi}$ and $P_{m,t}^{up,\phi}$ are respectively the lower and upper bounds of load demand confidence interval.

B. Power Flow Model

Both balanced and unbalanced distribution networks are the focus of this work, we thus employ a three-phase AC power flow model. At the first stage, the model determines HC, location, and size of SVC.

1) Power Flow Equation: Mutual impedance of branches is abandoned from impedance matrix because they are much smaller than the self-impedance [25], [30]. Therefore, a phase-decoupled power flow model is established. Let $\mathcal{I}$ be the set of all nodes, $V_{i,t}^{\phi}$ be the voltage magnitude of i-th node at t, and $\theta_{ij,t}^{\phi}$ be the phase angle difference between i and j at t. The net real and reactive power at node i of phase ϕ are

$$P_{i,t}^{\phi} = \sum_{j \in \mathcal{I}} V_{i,t}^{\phi} V_{j,t}^{\phi} \left(G_{ij}^{\phi} \cos\theta_{ij,t}^{\phi} + B_{ij}^{\phi} \sin\theta_{ij,t}^{\phi}\right), \forall t \in \mathcal{T}, \quad (5)$$

$$Q_{i,t}^{\phi} = \sum_{j \in \mathcal{I}} V_{i,t}^{\phi} V_{j,t}^{\phi} \left(G_{ij}^{\phi} \sin\theta_{ij,t}^{\phi} - B_{ij}^{\phi} \cos\theta_{ij,t}^{\phi}\right), \forall t \in \mathcal{T}, \quad (6)$$

where G_{ij}^{ϕ} and B_{ij}^{ϕ} denote respectively conductance and susceptance components of the admittance matrix.

2) Unit Constraints: We let $P_{n,t}^{pv,s,\phi}$, $Q_{n,t}^{pv,s,\phi}$, $\underline{\theta}_n^{pv,\phi}$ and $\overline{\theta}_n^{pv,\phi}$ represent the scheduled active power, reactive power, lower and upper limit of power factor angle of PV. Let $P_{l,t}^{g,\phi}$, $Q_{l,t}^{g,\phi}$, $C_l^{g,\phi}$, $\alpha_l^{p,\phi}$, $\alpha_l^{q,\phi}$, and $\theta_l^{g,\phi}$ denote the active power, reactive power, capacity, minimum output coefficient, coefficient of maximum phase-lead operation, and power factor angle for GTG, respectively. Let $\lambda_r^{svc,\phi}$ represent decision variable that indicates whether SVC is installed. Let $Q_{r,t}^{svc,\phi}$, $X^{svc,\phi}$, $C_r^{svc,\phi}$, and $\overline{C}_r^{svc,\phi}$ respectively denote reactive power,

number, capacity, and maximum allowable capacity for SVC. We formulate constraints as follows:

$$P_{n,t}^{pv,s,\phi} = k_{n,t}^{f,\phi} C_n^{pv,\phi}, \forall n \in \mathcal{N}, \forall t \in \mathcal{T}, \tag{7}$$

$$-P_{n,t}^{pv,s,\phi} \tan \underline{\theta}_n^{pv,\phi} \leq Q_{n,t}^{pv,s,\phi} \leq P_{n,t}^{pv,s,\phi} \tan \overline{\theta}_n^{pv,\phi}, \quad \forall n \in \mathcal{N}, \forall t \in \mathcal{T}, \tag{8}$$

$$\alpha_l^{p,\phi} C_l^{g,\phi} \leq P_{l,t}^{g,\phi} \leq C_l^{g,\phi}, \forall l \in \mathcal{L}, \forall t \in \mathcal{T}, \tag{9}$$

$$-\alpha_l^{q,\phi} C_l^{g,\phi} \leq Q_{l,t}^{g,\phi} \leq C_l^{g,\phi} \tan \theta_l^{g,\phi}, \forall l \in \mathcal{L}, \forall t \in \mathcal{T}, \tag{10}$$

$$-C_r^{svc,\phi} \leq Q_{r,t}^{svc,\phi} \leq C_r^{svc,\phi}, \forall r \in \mathcal{R}, \forall t \in \mathcal{T}, \tag{11}$$

$$0 \leq C_r^{svc,\phi} \leq \lambda_r^{svc,\phi} \overline{C}_r^{svc,\phi}, \lambda_r^{svc,\phi} \in \{0,1\}, \forall r \in \mathcal{R}, \tag{12}$$

$$\sum_{r \in \mathcal{R}} \lambda_r^{svc,\phi} = X^{svc,\phi}, \tag{13}$$

where $\mathcal{L}$ and $\mathcal{R}$ stand for sets of GTG and SVC, respectively. Constraint (7) represents the relation between the PV capacity and its output. Constraint (8) denotes that the reactive power of PV inverter can be adjusted within the predetermined range. GTG output is limited by (9) and (10). Constraint (11) represents lower and upper bounds of the reactive power SVC provides. Constraint (12) indicates that the SVC capacity is zero if it is not installed. Constraint (13) shows that the total number of installed SVCs is equal to $X^{svc,\phi}$. The ramping constraints, start-up and shut-down constraints, and minimum up and down time constraints of GTG are ignored due to its characteristics of fast start-up time and ramping.

3) Security Constraints: The overvoltage is a major concern that utilities have for high PV penetration [6], [11]. Following [6], [11], this paper considers the voltage limit as the security constraint when determining HC. Besides, line thermal capacity constraints are also considered and several linear box constraints are employed to approximate the quadratic constraint [25]. It is possible to consider other security constraints within the proposed model. The security limit is modeled as

$$\underline{V}^{\phi^2} \leq V_{i,t}^{\phi^2} \leq \overline{V}^{\phi^2}, \forall i \in \mathcal{I}, \forall t \in \mathcal{T}, \tag{14}$$

$$-\overline{S}_{ij}^{\phi} \leq P_{ij,t}^{\phi} \leq \overline{S}_{ij}^{\phi}, \forall (i,j) \in \mathcal{B}, \forall t \in \mathcal{T}, \tag{15}$$

$$-\overline{S}_{ij}^{\phi} \leq Q_{ij,t}^{\phi} \leq \overline{S}_{ij}^{\phi}, \forall (i,j) \in \mathcal{B}, \forall t \in \mathcal{T}, \tag{16}$$

$$-\sqrt{2}\overline{S}_{ij}^{\phi} \leq P_{ij,t}^{\phi} + Q_{ij,t}^{\phi} \leq \sqrt{2}\overline{S}_{ij}^{\phi}, \forall (i,j) \in \mathcal{B}, \forall t \in \mathcal{T}, \tag{17}$$

$$-\sqrt{2}\overline{S}_{ij}^{\phi} \leq P_{ij,t}^{\phi} - Q_{ij,t}^{\phi} \leq \sqrt{2}\overline{S}_{ij}^{\phi}, \forall (i,j) \in \mathcal{B}, \forall t \in \mathcal{T}, \tag{18}$$

where $\underline{V}$ and $\bar{V}$ are voltage lower and upper bounds. $\overline{S}_{ij}^{\phi}$ is the apparent power capacity of distribution line (i,j).

C. Uncertainty Accommodation

When the uncertainty is materialized, it is accommodated by the flexible resources in the system. This paper employs affine policy to implement the recourse actions of controllable resources to accommodate the uncertainty. Affine policy can be at least traced back to the 1950s in multi-stage stochastic programming [31], and is relevant to the linear controller in Control community. It provides closed-form control signal once uncertainty is materialized. In the power industry, a similar concept is adopted in AGC. Next, we model the recourse action with affine policy in the distribution network. Let $\boldsymbol{\epsilon_t} \in \mathbb{R}^{N_u}$ denote the PV output and load demand uncertainty vector. N_u is the length of the uncertainty vector. We then define the recourse action as

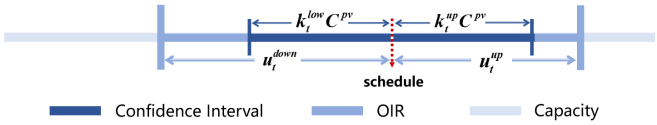

Fig. 2. Comparison of PV confidence interval, Optimal Injection Range (OIR), and capacity.

$$\begin{cases} \boldsymbol{y_t^P}(\boldsymbol{\epsilon_t}) \triangleq \boldsymbol{F_t^P}\boldsymbol{\epsilon_t}, \boldsymbol{y_t^Q}(\boldsymbol{\epsilon_t}) \triangleq \boldsymbol{F_t^Q}\boldsymbol{\epsilon_t}, \\ \boldsymbol{y_t^V}(\boldsymbol{\epsilon_t}) \triangleq \boldsymbol{F_t^V}\boldsymbol{\epsilon_t}, \boldsymbol{y_t^\theta}(\boldsymbol{\epsilon_t}) \triangleq \boldsymbol{F_t^\theta}\boldsymbol{\epsilon_t}, \end{cases} \quad \boldsymbol{\epsilon_t} \in \mathcal{U}_t, \forall t \in \mathcal{T}, \tag{19}$$

where $\boldsymbol{F_t^P}$, $\boldsymbol{F_t^Q}$, $\boldsymbol{F_t^V}$ and $\boldsymbol{F_t^\theta}$ are matrices that map uncertainty to changes of real power, reactive power, voltage magnitude, and phase angle, respectively. $\mathcal{U}_t$ is the uncertainty set to be determined together with HC, and is defined as

$$\mathcal{U}_t \triangleq \left\{ \boldsymbol{\epsilon_t} \in \mathbb{R}^{N_u} : -\boldsymbol{u_t^{down}} \leq \boldsymbol{\epsilon_t} \leq \boldsymbol{u_t^{up}} \right\}, \forall t \in \mathcal{T}, \tag{20}$$

where $\boldsymbol{u_t^{down}}$ and $\boldsymbol{u_t^{up}}$ denote the uncertainty downward and upward limit, respectively. When uncertainty $\boldsymbol{\epsilon_t}$ is materialized at Stage-2, $\boldsymbol{P_t} + \boldsymbol{y_t^P}(\boldsymbol{\epsilon_t})$, $\boldsymbol{Q_t} + \boldsymbol{y_t^Q}(\boldsymbol{\epsilon_t})$, $\boldsymbol{V_t} + \boldsymbol{y_t^V}(\boldsymbol{\epsilon_t})$, and $\boldsymbol{\theta_t} + \boldsymbol{y_t^\theta}(\boldsymbol{\epsilon_t})$ are new variables obtained, and they respect power flow equation (5)-(6), unit constraints (7)-(13), and security constraints (14)-(18).

As $\mathcal{U}_t$ is optimally determined, $\mathcal{U}_t$ is called Optimal Injection-Range (OIR). It is related to HC, and we formulate constraints as follows

$$P_{n,t}^{pv,s,\phi} + u_{n,t}^{up,\phi} \geq \left(k_t^{f,\phi} + k_t^{up,\phi} \right) C_n^{pv,\phi}, \forall n \in \mathcal{N}, \forall t \in \mathcal{T}, \tag{21}$$

$$P_{n,t}^{pv,s,\phi} - u_{n,t}^{down,\phi} \leq \left(k_t^{f,\phi} - k_t^{low,\phi} \right) C_n^{pv,\phi}, \forall n \in \mathcal{N}, \quad \forall t \in \mathcal{T}, \tag{22}$$

$$u_{m,t}^{up,\phi} \geq P_{m,t}^{up,\phi}, \forall m \in \mathcal{M}, \forall t \in \mathcal{T}, \tag{23}$$

$$u_{m,t}^{down,\phi} \geq P_{m,t}^{low,\phi}, \forall m \in \mathcal{M}, \forall t \in \mathcal{T}, \tag{24}$$

which guarantee that PV output and load demand in the confidence interval can always be accommodated in OIR. Fig. 2 illustrates the relationship between uncertainty, confidence interval, and OIR of PV.

With aforementioned constraints, the uncertainty-proof HC can be obtained by solving the optimization problem below

$$\text{(P)} \quad \max \sum_{n \in \mathcal{N}} C_n^{pv,\phi}$$
$$\text{s.t.} \quad (5) - (24).$$

We will show how to solve problem (P) in short. As a side note, the investment cost can be added to the model if necessary, and the solution techniques still apply. It is also possible to model other equipment, such as online tap changer (OLTC).

III. A Hybrid Relaxation based Solution Approach

The proposed adjustable model (P) is a nonlinear programming problem. First, the power flow model is nonlinear and nonconvex. Second, the affine recourse action at the second stage has introduced more nonlinear terms. Third, the model has variable uncertainty set that is relevant to HC. To overcome these challenges, we propose a novel hybrid relaxation solution approach in this section. The basic idea is to use strong relaxation techniques at Stage-1 to get (near) exact solution for the output schedule. At Stage-2, we propose a linearized power flow model at the point attained from Stage-1. The rationale of the hybrid relaxation is to provide a good nominal point for linearization, which is used both in affine policy and power flow approximation.

A. Second Order Cone Relaxation at Stage-1

At the first stage, the second-order cone (SOC) relaxation is employed to convexify the nonconvex terms. SOC relaxation is an effective tool to convexify the regular power flow model in radial distribution networks [32] [33]. For self-contained reasons, we present SOC relaxation here. By introducing

$$W_{i,t}^{\phi} \triangleq {V_{i,t}^{\phi}}^2/\sqrt{2}, \qquad \forall i \in \mathcal{I}, \forall t \in \mathcal{T} \tag{25}$$

$$R_{ij,t}^{\phi} \triangleq V_{i,t}^{\phi} V_{j,t}^{\phi} \cos\theta_{ij,t}^{\phi}, \quad \forall i \in \mathcal{I}, \forall t \in \mathcal{T} \tag{26}$$

$$T_{ij,t}^{\phi} \triangleq V_{i,t}^{\phi} V_{j,t}^{\phi} \sin\theta_{ij,t}^{\phi}, \quad \forall i \in \mathcal{I}, \forall t \in \mathcal{T}, \tag{27}$$

we rewrite (5) and (6) as

$$P_{i,t}^{\phi} = \sum_{j \in \mathcal{I}} \left(G_{ij}^{\phi} R_{ij,t}^{\phi} + B_{ij}^{\phi} T_{ij,t}^{\phi} \right), \forall t \in \mathcal{T}, \tag{28}$$

$$Q_{i,t}^{\phi} = \sum_{j \in \mathcal{I}} \left(G_{ij}^{\phi} T_{ij,t}^{\phi} - B_{ij}^{\phi} R_{ij,t}^{\phi} \right), \forall t \in \mathcal{T}, \tag{29}$$

$$R_{ij,t}^{\phi^2} + T_{ij,t}^{\phi^2} = 2 W_{i,t}^{\phi} W_{j,t}^{\phi}, \forall t \in \mathcal{T}. \tag{30}$$

The flow equations (28) and (29) are linear in $R_{ij,t}^{\phi}$ and $T_{ij,t}^{\phi}$. We relax (30) to a inequality constraint as

$$R_{ij,t}^{\phi^2} + T_{ij,t}^{\phi^2} \leq 2 W_{i,t}^{\phi} W_{j,t}^{\phi}, \forall t \in \mathcal{T}. \tag{31}$$

B. Linearization at Stage-2

Although SOC relaxation works well in regular power flow problems, it becomes difficult to convexify the recourse action (19) when considering the uncertainty. In the power community, linearized power flow models with high accuracy recently gain much attention [34]. They are attractive as linear models often have good computational performance. In order to capture the recourse action at Stage-2, we propose a novel linearized power flow model that integrates SOC relaxation. The rationale is to leverage the accuracy of SOC relaxation for both linearization and affine policy. In fact, affine policy has close relation with the first-order Taylor expansion, especially when the uncertainty is small. Inspired by [34]–[36], we present two assumptions as follows.

Assumption 1. *Voltage phase angle difference at two connected nodes is "small".*

Assumption 2. *Voltage magnitude is close to 1.0 p.u..*

They are true in general for the distribution network. Following these two assumptions, we have

$$\cos\theta_{ij,t}^{\phi} \approx 1 - \frac{1}{2}\theta_{ij,t}^{\phi^2}, \tag{32}$$

$$V_{i,t}^{\phi} V_{j,t}^{\phi} \theta_{ij,t}^{\phi^2} \approx \theta_{ij,t}^{\phi^2}, \tag{33}$$

$$\theta_{ij,t}^{\phi} \approx V_{i,t}^{\phi} V_{j,t}^{\phi} \sin\theta_{ij,t}^{\phi}. \tag{34}$$

Let the nominal point be $\left(V_{i,t}^{\phi^{(0)}}, \theta_{ij,t}^{\phi^{(0)}}\right)$, which are known. We establish the proposition below to linearize the power flow model.

Proposition 1. *Given nominal point, the KCL equation with uncertainty can be approximated by*

$$\hat{P}_{i,t}^{\phi}(\boldsymbol{\epsilon_t}) = \sum_{j \in \mathcal{I}} \Bigg(G_{ij}^{\phi} \frac{\hat{W}_{i,t}^{\phi}(\boldsymbol{\epsilon_t}) + \hat{W}_{j,t}^{\phi}(\boldsymbol{\epsilon_t})}{\sqrt{2}} + B_{ij}^{\phi} \hat{T}_{ij,t}^{\phi}(\boldsymbol{\epsilon_t})$$
$$- G_{ij}^{\phi} \Bigg(\sqrt{2} \frac{V_{i,t}^{\phi^{(0)}} - V_{j,t}^{\phi^{(0)}}}{V_{i,t}^{\phi^{(0)}} + V_{j,t}^{\phi^{(0)}}} \left(\hat{W}_{i,t}^{\phi}(\boldsymbol{\epsilon_t}) - \hat{W}_{j,t}^{\phi}(\boldsymbol{\epsilon_t}) \right) - \frac{1}{2} {\theta_{ij,t}^{\phi^{(0)}}}^2$$
$$+ \theta_{ij,t}^{\phi^{(0)}} \hat{T}_{ij,t}^{\phi}(\boldsymbol{\epsilon_t}) - \frac{1}{2} \left(V_{i,t}^{\phi^{(0)}} - V_{j,t}^{\phi^{(0)}} \right)^2 \Bigg) \Bigg), \forall t \in \mathcal{T}, \tag{35}$$

$$\hat{Q}_{i,t}^{\phi}(\boldsymbol{\epsilon_t}) = \sum_{j \in \mathcal{I}} \Bigg(-B_{ij}^{\phi} \frac{\hat{W}_{i,t}^{\phi}(\boldsymbol{\epsilon_t}) + \hat{W}_{j,t}^{\phi}(\boldsymbol{\epsilon_t})}{\sqrt{2}} + G_{ij}^{\phi} \hat{T}_{ij,t}^{\phi}(\boldsymbol{\epsilon_t})$$
$$+ B_{ij}^{\phi} \Bigg(\sqrt{2} \frac{V_{i,t}^{\phi^{(0)}} - V_{j,t}^{\phi^{(0)}}}{V_{i,t}^{\phi^{(0)}} + V_{j,t}^{\phi^{(0)}}} \left(\hat{W}_{i,t}^{\phi}(\boldsymbol{\epsilon_t}) - \hat{W}_{j,t}^{\phi}(\boldsymbol{\epsilon_t}) \right) - \frac{1}{2} {\theta_{ij,t}^{\phi^{(0)}}}^2$$
$$+ \theta_{ij,t}^{\phi^{(0)}} \hat{T}_{ij,t}^{\phi}(\boldsymbol{\epsilon_t}) - \frac{1}{2} \left(V_{i,t}^{\phi^{(0)}} - V_{j,t}^{\phi^{(0)}} \right)^2 \Bigg) \Bigg), \forall t \in \mathcal{T}. \tag{36}$$

Proof. By substituting (32) and (33) into (5) and (6), we have the following equations:

$$P_{i,t}^{\phi} \approx \sum_{j \in \mathcal{I}} \Bigg(G_{ij}^{\phi} \frac{V_{i,t}^{\phi^2} + V_{j,t}^{\phi^2}}{2} + B_{ij}^{\phi} V_{i,t}^{\phi} V_{j,t}^{\phi} \sin\theta_{ij,t}^{\phi}$$
$$- \frac{G_{ij}^{\phi}}{2} \left(V_{ij,t}^{\phi^2} + \theta_{ij,t}^{\phi^2} \right) \Bigg), \forall t \in \mathcal{T}, \tag{37}$$

$$Q_{i,t}^{\phi} \approx \sum_{j \in \mathcal{I}} \Bigg(-B_{ij}^{\phi} \frac{V_{i,t}^{\phi^2} + V_{j,t}^{\phi^2}}{2} + G_{ij}^{\phi} V_{i,t}^{\phi} V_{j,t}^{\phi} \sin\theta_{ij,t}^{\phi}$$
$$+ \frac{B_{ij}^{\phi}}{2} \left(V_{ij,t}^{\phi^2} + \theta_{ij,t}^{\phi^2} \right) \Bigg), \forall t \in \mathcal{T}, \tag{38}$$

where $V_{ij,t}^{\phi^2} = \left(V_{i,t}^{\phi} - V_{j,t}^{\phi} \right)^2$. We then establish following equations

$$\theta_{ij,t}^{\phi^2} \approx 2\theta_{ij,t}^{\phi^{(0)}} \theta_{ij,t}^{\phi} - {\theta_{ij,t}^{\phi^{(0)}}}^2 \approx 2\theta_{ij,t}^{\phi^{(0)}} V_{i,t}^{\phi} V_{j,t}^{\phi} \sin\theta_{ij,t}^{\phi} - {\theta_{ij,t}^{\phi^{(0)}}}^2, \tag{39}$$

$$V_{ij,t}^{\phi^2} \approx 2V_{ij,t}^{\phi^{(0)}} V_{ij,t}^{\phi} - {V_{ij,t}^{\phi^{(0)}}}^2 \approx 2V_{ij,t}^{\phi^{(0)}} \frac{V_{i,t}^{\phi^2} - V_{j,t}^{\phi^2}}{V_{i,t}^{\phi^{(0)}} + V_{j,t}^{\phi^{(0)}}} - {V_{ij,t}^{\phi^{(0)}}}^2 \tag{40}$$

The first and third approximations follow Assumption 1 and the first-order Taylor expansion, and the second approximation is from (34). According to Assumption 2, the last approximation follows $V_{ij,t}^{\phi} = V_{i,t}^{\phi} - V_{j,t}^{\phi} \approx (V_{i,t}^{\phi} - V_{j,t}^{\phi})(V_{i,t}^{\phi}+V_{j,t}^{\phi})/(V_{i,t}^{\phi^{(0)}}+V_{j,t}^{\phi^{(0)}})$. By replacing $V_{i,t}^{\phi}V_{j,t}^{\phi}\sin\theta_{ij,t}^{\phi}$ and $V_{i,t}^{\phi^2}/\sqrt{2}$ with $T_{ij,t}^{\phi}$ and $W_{i,t}^{\phi}$, respectively, and substituting (39) and (40) into (37) and (38), we obtain the proposed linearized power flow equations. □

C. Surrogate Affine Approximation

As the PV capacity is to be determined, the uncertainty set for PV output is variable in problem (P). Regular affine policy based methods thus cannot solve it directly. For notation simplicity, we rewrite the relaxed model in compact form

$$\text{(P1)} \quad \max_{\boldsymbol{x},\boldsymbol{z},\boldsymbol{F}} \ \boldsymbol{c}^{\boldsymbol{T}}\boldsymbol{x} \tag{41}$$

$$\text{s.t.} \quad \boldsymbol{A}\boldsymbol{x} + \boldsymbol{N}\boldsymbol{z} \le \boldsymbol{h}, \tag{42}$$

$$\|\boldsymbol{K}_b\boldsymbol{z}\|_2 \le \boldsymbol{J}_b\boldsymbol{z}, \forall b \in \mathcal{B}, \tag{43}$$

$$\boldsymbol{B}\boldsymbol{x} + \boldsymbol{E}\boldsymbol{\epsilon} + \boldsymbol{S}\boldsymbol{z} + \boldsymbol{C}^P\boldsymbol{y}^P(\boldsymbol{\epsilon}) + \boldsymbol{C}^Q\boldsymbol{y}^Q(\boldsymbol{\epsilon}) + \boldsymbol{C}^z\boldsymbol{y}^z(\boldsymbol{\epsilon}) \le \boldsymbol{d}, \forall \boldsymbol{\epsilon} \in \mathcal{U}, \tag{44}$$

where $\boldsymbol{x}$ includes capacity and scheduled output of DER, location of SVC, and OIR. The variable $\boldsymbol{z}$ includes auxiliary variables (25)-(27). Equation (7)–(18), (21)-(24), (28) and (29) are rewritten in (42). (31) is represented by (43). Equation (35)-(36), unit constraints and security constraints at the second stage are rewritten in (44). Although the SOC and linearization reduce the non-linearity, the relaxed model is still computationally intractable due to the variable uncertainty set $\mathcal{U}$ and affine policy in equation (44).

We employ the Surrogate Affine Approximation (SAA) method to replace the variable uncertainty set with a deterministic one [28]. First, we introduce a set of surrogate variables

$$\mathbf{0} \le \boldsymbol{\delta}^{\text{LB}} \le \mathbf{1}, \quad \mathbf{0} \le \boldsymbol{\delta}^{\text{UB}} \le \mathbf{1},$$

and a surrogate function

$$\boldsymbol{s}(\boldsymbol{U}^{\text{LB}}, \boldsymbol{U}^{\text{UB}}) \triangleq \boldsymbol{U}^{\text{UB}}\boldsymbol{\delta}^{\text{UB}} - \boldsymbol{U}^{\text{LB}}\boldsymbol{\delta}^{\text{LB}}, \tag{45}$$

where $\boldsymbol{U}^{\text{LB}} = \text{diag}\left(\boldsymbol{u}^{\boldsymbol{down}}\right)$ and $\boldsymbol{U}^{\text{UB}} = \text{diag}\left(\boldsymbol{u}^{\boldsymbol{up}}\right)$. Equation (44) is then recast as

$$\boldsymbol{B}\boldsymbol{x} + \boldsymbol{S}\boldsymbol{z} + \boldsymbol{\pi}\cdot\mathbf{1} \le \boldsymbol{d}, \tag{46}$$

$$\boldsymbol{C}^{\boldsymbol{P}}\hat{\boldsymbol{F}}^{\boldsymbol{P}} + \boldsymbol{C}^{\boldsymbol{Q}}\hat{\boldsymbol{F}}^{\boldsymbol{Q}} + \boldsymbol{C}^{\boldsymbol{z}}\hat{\boldsymbol{F}}^{\boldsymbol{z}} + \boldsymbol{E}[-\boldsymbol{U}^{\text{LB}}, \boldsymbol{U}^{\text{UB}}] \le \boldsymbol{\pi}, \tag{47}$$

$$\boldsymbol{\pi} \ge \mathbf{0}, \tag{48}$$

where $\boldsymbol{\pi}$ is a matrix of non-negative multipliers. $\hat{\boldsymbol{F}}^{\boldsymbol{P}}$, $\hat{\boldsymbol{F}}^{\boldsymbol{Q}}$ and $\hat{\boldsymbol{F}}^{\boldsymbol{z}}$ are new surrogate matrices. The hybrid relaxation model is thus formulated as

$$\text{(P2)} \quad \max_{\boldsymbol{x},\boldsymbol{z},\hat{\boldsymbol{F}},\boldsymbol{\pi}} \ \boldsymbol{c}^{\boldsymbol{T}}\boldsymbol{x}$$

$$\text{s.t.} \quad (42)-(43), (46)-(48).$$

(P2) is an SOC problem, and can be solved efficiently using the off-the-shelf solvers.

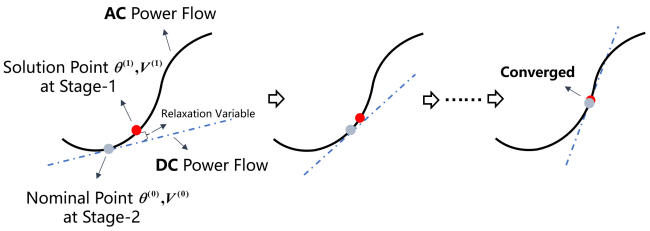

Fig. 3. Hybrid model with SOC relaxation at Stage-1 and linearization at Stage-2. Nominal point for linearization approximates to the solution point with iterations.

Algorithm 1 Successive Hybrid Relaxation Algorithm

Input: N_k: maximum iteration time; Δ: maximum L2 norm
Output: optimal $\boldsymbol{x}^*$, $\boldsymbol{z}^*$, $\hat{\boldsymbol{F}}^*$, $\boldsymbol{\pi}^*$

```
Initialization: v^(1) ← 1, θ^(1) ← 0, δ^(1) ← ∞, k ← 1
while k < N_k or δ^(k) ≥ Δ do
    Update nominal point (v^(0), θ^(0)) ← (v^(k), θ^(k))
    Linearize power flow at Stage-2 based on (35)-(36)
    Formulate problem (P2)
    Solve (P2), get (x^(k+1), z^(k+1), F^(k+1), π^(k+1))
    Extract (v^(k+1), θ^(k+1)) from z^(k+1)
    δ^(k+1) ← ||(v^(k+1) − v^(k), θ^(k+1) − θ^(k))||_2;
    k ← k + 1;
end while
```

D. Successive Hybrid Relaxation Algorithm

The linear power flow (35)-(36) at Stage-2 is linearized at the nominal point based on Taylor approximation. However, the solution point may be different from the nominal point. In the meantime, the solution point also serves as the base point for the uncertainty accommodation, and the affine matrix is an analogy to the gradient in Taylor approximation. We present a successive hybrid relaxation algorithm below to find the converged solution and nominal point. Fig. 3 illustrates the basic idea. The nominal point approximates to the solution point with iterations.

In Algorithm 1, SOC problem (P2) is iteratively solved. The nominal point is updated with the voltage information extracted from the solution to (P2).

IV. Case Study

The simulations are performed with a single-phase 141-node distribution feeder of nominal voltage 12.47 kV [37] and a three-phase IEEE 33-bus distribution feeder of nominal voltage 12.66 kV [38]. Typical load and PV profiles are from [39]. The load curves and PV forecast are obtained based on the average value of hourly historical data. Without loss of generality, assume uncertainty around forecast value follows Gaussian distribution, and we use the 95% confidence interval of PV and load deviation. All cases are carried out in a server with Intel(R) Xeon(R) Gold 6140 (2.30 GHz). The proposed solution approach is programmed in Matlab 2021b and solved by Mosek 9.3.

A. Single-phase 141-node Test System

Fig. 4 illustrates the single-line diagram of the 141-node distribution feeder. The feeder includes 84 load nodes with

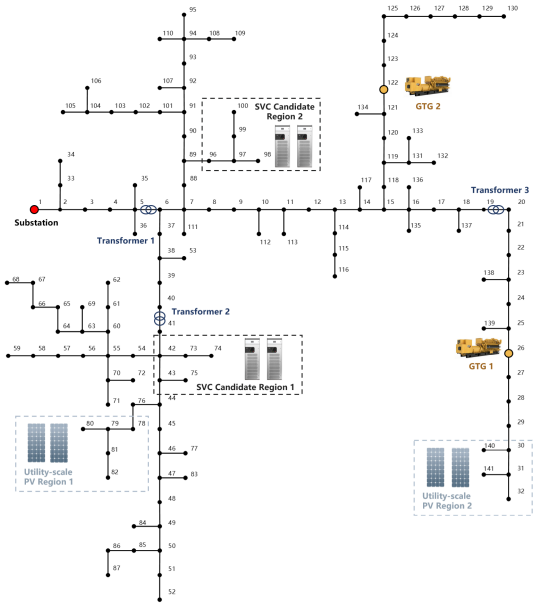

Fig. 4. Single-line diagram of the 141-node distribution feeder. The location and size of SVC are determined among the SVC candidate regions. The placement and parameters of GTG are predefined.

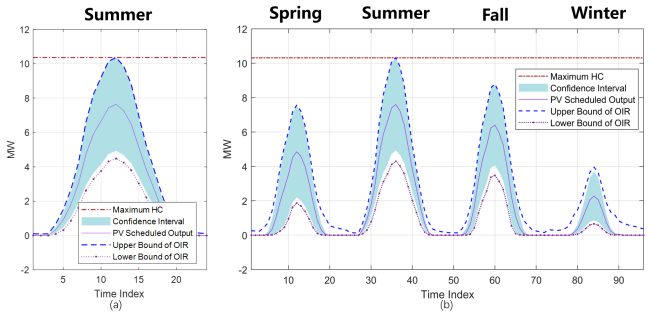

Fig. 5. PV scheduled output, HC, OIR and the confidence interval obtained by the proposed model under (a) typical day for summer (b) four typical days for various seasons.

the peak being 11.9 MW and 7.4 MVar. The lower and the upper voltage limits are set as 0.95 p.u. and 1.05 p.u., respectively. Line thermal limits are relaxed in this system due to their abundant capacity. Utility-scale PVs are installed at node 30, 31, 32, 140, 141, 78, 79, 80, 81, and 82. Each PV system is assumed to operate at the unity power factor. Two SVCs are installed at two nodes out of node 42, 43, 73, 74, 75, 96, 97, 98, 99, and 100. The voltage ratios of three transformers are set to 1:1.04, 1:1.015 and 1:1.035, respectively. In this simulation, GTGs already deployed in the system are dispatched to increase uncertainty-proof HC. Thus, the placement and parameters of GTG are predefined. Node 26 and 122 are with GTGs.

In this part, we first analyze uncertainty-proof HC results obtained from the proposed approach with PV output uncertainty, and then investigate the convergence performance. Sensitivity studies are then performed to check the impact on HC from SVC and GTG. Next, to check the accuracy and HC improvement, we compare the result of the proposed model and other methods. Finally, the impact of load uncertainty is discussed.

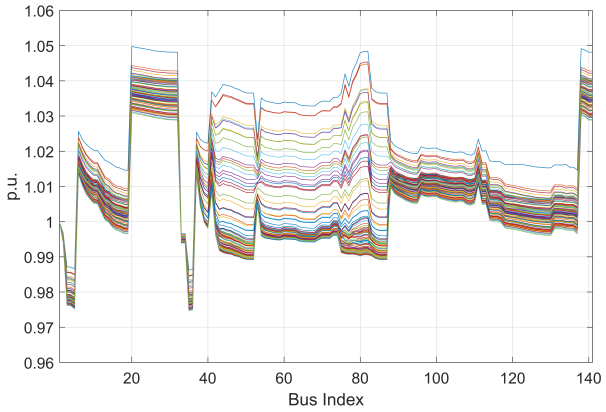

Fig. 6. Voltage profile in the worst-case scenario where PV out deviate from forecast value to the upper bound of OIR. (96 profiles for t=1 to 96).

1) Uncertainty-proof HC: Fig. 5(a) presents the converged result of HC, PV scheduled output, and OIR in summer. The attained uncertainty-proof HC is 10.3MW, which is 86.6% of annual peak load. The figure shows that the confidence interval of PV output is always within OIR. It indicates that any PV output uncertainty within the confidence interval can be mitigated by re-dispatch actions. The minimum net load is -0.5 MW at 12:00 (i.e., -0.5 MW = the load of 9.8 MW - PV output of 10.3 MW), and it is equal to the sum of network loss and minimum GTG output. PV power output will be curtailed if HC continues to increase. Thus, the uncertainty-proof HC obtained by the proposed model is maximal. On the other hand, we also perform the simulations for various seasons, and the result is shown in Fig. 5(b). It is observed that HC is almost the same as that attained for summer. That shows the summer net load is a dominant factor in determining HC in this case. Besides, the solution time for summer season is about 190s, which is approximately 62% lower than that for all seasons. Hence, utility can get the HC quickly by considering the summer season only.

Fig. 6 illustrates the voltage profile of four seasons after re-dispatch in the worst-case scenario, in which the PV output deviates from a forecast value to the upper bound of OIR. It is observed that voltage magnitudes range from 0.97 to 1.05 and no over-voltage issue occurs. It again validates any uncertainty of PV output can be handled by the proposed recourse action without overvoltage violation. Thus, utility can use the explicit policy directly to dispatch SVCs and GTGs when PV uncertainty is materialized, and optimal power flow is eliminated in the process of re-dispatch.

As a side note, integer constraints for the SVC location are relaxed first and then enforced to speed up solving time. Node 43 and 75 are selected for SVC siting by the model, and their capacities are determined as 2.43 MVar and 3.90 MVar, respectively.

2) Convergence Performance: To illustrate the convergence of the algorithm, Fig. 7 presents the Euclidean distance (L2 norm) curve versus iteration number and the comparison of nominal point and converged solution. It is noted that the norm includes all nodes and periods. As shown in (a), the distance decreases with iteration in general. The proposed

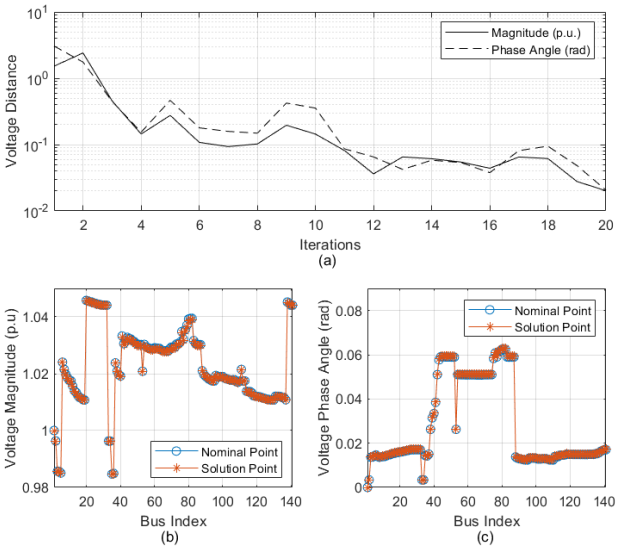

Fig. 7. Euclidean distance between the nominal and solution point with iteration and the comparison of the nominal point and converged solution point. (a) Euclidean distance, (b) Voltage magnitude, (c) Voltage phase angle.

TABLE I
CASES FOR SENSITIVITY ANALYSIS WITH DIFFERENT SIZES AND LOCATIONS OF GTG AND SVC

	GTG1 Loc.	GTG2 Loc.	SVC Loc.	GTG1 Cap.	GTG2 Cap.	SVC Cap.
Case 1	26	122	43	0MW	0MW	0-4MVar
Case 2	26	122	43	2.05MW	2.05MW	0-4MVar
Case 3	95	122	43	2.05MW	2.05MW	0-4MVar
Case 4	26	122	96	0MW	0MW	0-4MVar
Case 5	26	122	96	2.05MW	2.05MW	0-4MVar

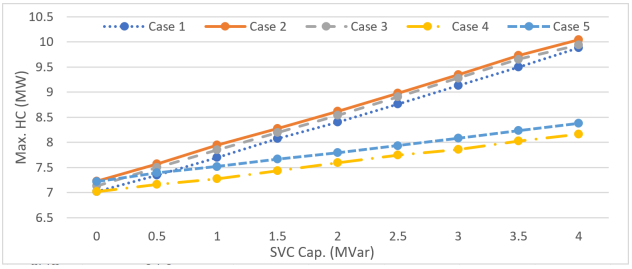

Fig. 8. HC versus SVC with different cases.

successive hybrid relaxation algorithm takes 20 iterations to get the converged solution. The voltage magnitude distance reduces about 99% (i.e., (1.25 - 0.012)/1.25, and the phase angle distance decreases by 99% (i.e., (1.58-0.012)/1.58≈99%). After it converges, the solution point is close to the nominal point. (b) and (c) show the detailed voltage magnitude and phase angle curves comparison for all nodes at period 36. The largest voltage magnitude gap is 0.00056 p.u and angle gap is 0.00037 rad.

3) Sensitivity Analysis: The sensitivity studies are performed to investigate the impact on HC value from GTG and SVC size and location. As shown in Fig. 4, utility-scale PVs are installed in the two utility-scale PV regions. Case studies shown in Table I were performed. In Fig. 8, five different

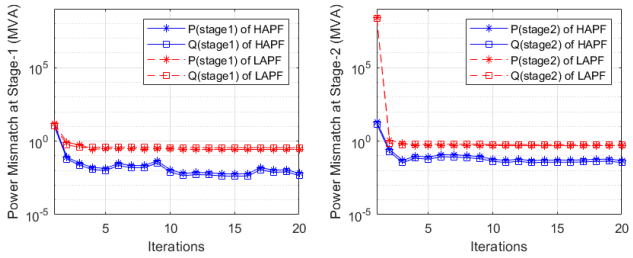

Fig. 9. The convergence comparison of HAPF and LAPF models. Power mismatch at Stage-1 (left). Power mismatch at Stage-2 (right).

curves represent the maximum HC solved by the proposed model versus SVC with different cases, respectively. It is observed that curves of cases 1, 2, 3 and curves of cases 4, 5 are close to each other, respectively. It indicates that HC value change is small even GTG capacity has a change of 4.1 MW with different locations. For instance, adding two GTGs increases HC by about 0.22 MW (i.e., 8.62 MW – 8.40 MW = 0.22 MW). On the other hand, the curve of case 1 shows that HC increases about 29% (i.e. (9.9-7.0)/9.9) when SVC capacity grows from 0 MVar to 4 MVar. The curves of cases 2 and 3 present similar results. Furthermore, the location of SVC also affects the maximum HC. As shown in the curves of case 4, the increase of HC is reduced to about 15% (i.e. (8.2-7.0)/8.2) when SVC is located far away from PV regions. It indicates HC is more sensitive to the SVC capacity and location. The reason is that SVC can provide flexible reactive power support to lower the voltage caused by PV generation. The closer SVC is located to the PV regions, the greater its effect on improving maximum HC.

From utility perspective, this analysis also offers a method to guide the planning department to determine maximum HC with different SVC sizes. From Fig.8, there is a positive correlation between the maximum HC and SVC size. Utilities can obtain the maximum HC directly according to two other results of maximum HC with different SVC sizes.

4) Comparison of Power Mismatch: The comparison of model accuracy is performed for the proposed hybrid adjustable power flow model (HAPF) and linearized adjustable power flow (LAPF). In the LAPF model, linearized power flow (35)-(36) is used at both Stage-1 and -2. The same placement of PV, GTG, SVC, load and test feeder mentioned in Fig.4 is used for both HAPF and LAPF.

To compare the accuracy, we calculate the power mismatch based on the exact Kirchhoff's Current Law (KCL) and Kirchhoff's Voltage Law (KVL) equations for each iteration, respectively. It is noted that the norm of power mismatch includes all nodes at the 36th period as an instance. As for Stage-2, to compare the power mismatch, assuming that PV uncertainty are both equal to 2.50 MW for HAPF and LAPF, and then the re-dispatch of controllable resources is obtained by $\hat{\boldsymbol{F}}$. The real and reactive power mismatches are illustrated in Fig. 9. It is observed that both HAPF and LAPF models can quickly converge at Stage-1 and -2. According to the figure on the left, the HAPF almost converges after four iterations at Stage-1, and LAPF also reaches its minimum power mismatch

TABLE II
THE COMPARISON OF HC SOLVED BY MONTE CARLO BASED METHODS AND HAPF IN DIFFERENT SVC CAPACITY AND GTG CAPACITY

SVC(MVar)	Min. HC*		Max. HC*		Max. HC**		Max.HC***		Max.HC****	
	GTG(MW)		GTG(MW)		GTG(MW)		GTG(MW)		GTG(MW)	
	0	4.1	0	4.1	0	4.1	0	4.1	0	4.1
0	1.436	1.461	6.818	6.821	6.823	6.828	7.018	7.225	7.055	7.284
0.5	1.436	1.495	6.846	6.862	7.144	7.278	7.346	7.569	7.414	7.639
1	1.467	1.557	6.881	7.012	7.485	7.727	7.698	7.944	7.770	8.002
1.5	1.467	1.590	6.881	7.190	7.796	8.098	8.072	8.278	8.129	8.349
2	1.478	1.601	6.931	7.258	7.863	8.243	8.401	8.619	8.494	8.728
2.5	1.503	1.660	7.076	7.273	8.549	8.590	8.760	8.978	8.862	9.087
3	1.543	1.705	7.296	7.517	8.756	9.058	9.127	9.349	9.230	9.467
3.5	1.607	1.778	7.557	7.794	9.220	9.315	9.501	9.728	9.620	9.841
4	1.643	1.787	7.823	8.047	9.639	9.859	9.880	10.045	9.999	10.139

[*] HC solved by PFCMC; [**] HC solved by OPFMC; [***] HC solved by HAPF; [****] HC solved by OPFMC based on HAPF.

at iteration 4. The figure on the right shows similar results for convergence speed. The figure shows that HAPF outperforms LAPF in terms of accuracy by about one order of magnitude. The L2 norm of HAPF mismatch at Stage-1 is less than 0.01 MW. In contrast, the mismatch of LAPF model is about 0.3 MW. The proposed HAPF reduces the mismatch by more than 90%. It shows similar trends at Stage-2 according to the figure on the right of Fig. 9. That is mainly because HAPF has better accuracy at Stage-1, which also provides a better nominal point for linearization and uncertainty accommodation at Stage-2.

5) HC Comparison via Monte Carlo Simulation: We compare the proposed HAPF with two Monte Carlo based methods below:

- Power Flow Calculation based Monte Carlo (PFCMC) simulation for HC evaluation, in which controllable resources are static;
- Optimal Power Flow based Monte Carlo (OPFMC) simulation for HC evaluation, in which controllable resources are adjustable.

The same placement of PV, GTG, SVC, load and test feeder mentioned in case 2 of sensitivity analysis is used as an instance.

PFCMC: The algorithm in [11] is used. A massive sampling of PV deployment scenarios is generated in multi-time series. The voltage magnitude is regarded as the security limit. By solving multi-period power flow, we get the maximum voltage in each PV deployment scenario of different PV penetration.

Fig. 10 shows the results of maximum node voltages for all PV deployments in the system without GTG and SVC. The hosting capacity is estimated based on 2500 PV deployment scenarios. From Fig. 10, when PV penetration exceeds 1.436 MW, overvoltage occurs in some PV configuration scenarios, as shown at point A. Additionally, all PV deployment scenarios cause violation if the penetration exceeds 6.818 MW at point B. Therefore, in the evaluation of PFCMC simulation algorithm, the minimum and maximum HC are 1.436 MW and 6.818 MW, respectively. In contrast, HAPF finds an HC of 7.018 MW in the same system. More importantly, there will be no voltage or unit violations with recourse action.

Table II presents minimum and maximum HCs solved by Monte Carlo based methods and HAPF in different SVC and GTG. The first column lists different SVC capacities, and column 2-11 presents HCs with various GTG capacities.

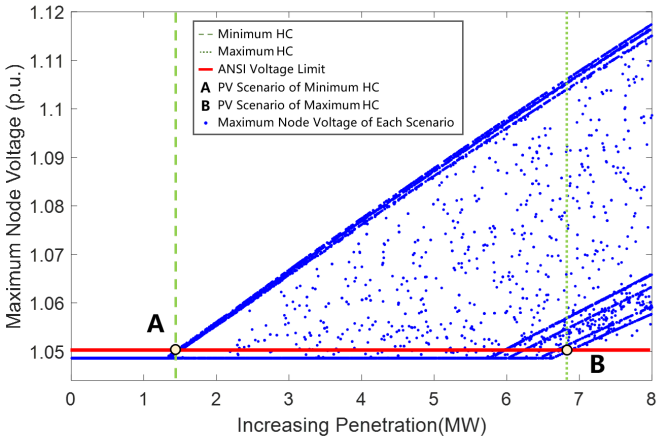

Fig. 10. Maximum node voltages for multiple PV deployment scenarios.

For example, column-3 shows the minimum HC solved by PFCMC with GTG capacity of 4.1 MW. It is observed that in general HC increases as the size of SVC and GTG become larger. For example, when SVC is 1 MVar, adding 4.1 MW GTG increases minimum HC from 1.467 MW to 1.557 MW. However, the maximum HC from PFCMC is smaller than that from HAPF in all cases. That is mainly because that the controllable resources are static in PFCMC, while they are adjustable by re-dispatch in HAPF.

OPFMC: In this part, an OPFMC simulation is to determine the maximum HC. The purpose of this simulation is to adjust GTG and SVC to avoid voltage limit violations.

Comparing column-4 to -5 and column-6 to -7 of Table II, OPFMC provides larger maximum HC than PFCMC. That is mainly because OPFMC can optimize the output of controllable resources to obtain a better maximum HC than PFCMC. However, HC from OPFMC is still smaller than that from HAPF. That is mainly because OPFMC's optimality is limited by its PV deployment scenarios while HAPF finds the near-optimal solution in the first place. Fig.11 shows the result of maximum HC from OPFMC with the increasing scenario numbers. It shows that the maximum HC improves in the first 1500 scenarios. However, the maximum HC remains almost unchanged after 2000 scenarios.

Furthermore, to verify the result of HAPF, the "optimal PV deployment" in HAPF is fed to OPFMC. OPFMC with

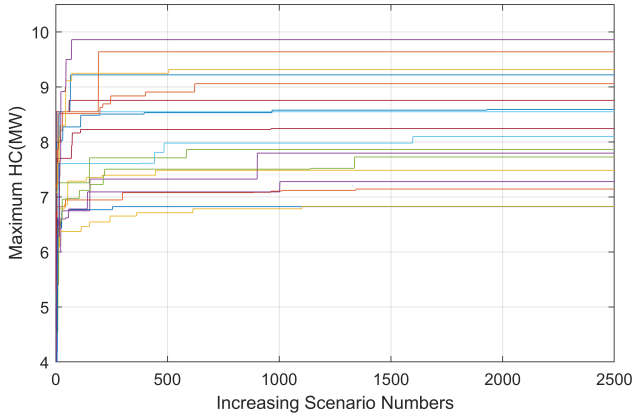

Fig. 11. Maximum HC for increasing scenario number of OPFMC (18 profiles for 18 cases of different size of SVC and GTG).

2000 scenarios is performed again based on the deployment of HAPF to find a larger HC. According to column-10 and -11 of Table II, the result is almost equal to the maximum HC of HAPF. Hence, the HC and linearized re-dispatch of HAPF are near-optimal. Utility can also use this strategy to guide the existing methods in determining the maximum HC.

In summary, the advantages of HAPF over Monte Carlo based methods include higher maximum HC, readily determined re-dispatch policy, and the optimal placement of SVC. As a side note, the dispatch policy of OPFMC is not available as the materialized uncertainty is nearly impossible to match these random scenarios exactly. In contrast, the dispatch policy of HAPF is closed-form function of uncertainty, and respects physical and security constraints. However, the solution time of HAPF in each iteration is about 500s. In contrast, parallel computing techniques can be easily applied in Monte Carlo based methods with thousands of samples, and one sample takes about 3s only.

6) Impact of Load Uncertainty: To analyze the impact of load uncertainty, simulation with load uncertainty is performed. The same placement of PV, GTG, SVC, load forecast and test feeder mentioned in case 2 of sensitivity analysis is used as an instance. Time resolution is set to 2 h in this part to reduce the model size. We will report generalized techniques to speed up optimization approach in future work.

Fig.12 (a) and (b) show the voltage profiles in the worst-case scenario. The worst-case scenario is defined as the scenario with the smallest net load, i.e., the highest PV power output and lowest load demand in this paper. We get HC of 8.71 MW when the load uncertainty is not considered. As shown in Fig.12 (a), the largest voltage magnitude is 1.06 in the worst-case scenario. It indicates ignorance of load uncertainty may lead to overvoltage. When load uncertainty is considered, HC attained by HAPF is 5.04 MW, which is about 58% (i.e., 58% = 5.04/8.71) of that not considering load uncertainty. Its voltage profile is depicted in Fig.12 (b). The highest voltage magnitude is 1.05 in Fig.12 (b). In other words, there is no overvoltage. It indicates that HAPF considering load uncertainty is more robust in dealing with the uncertainties.

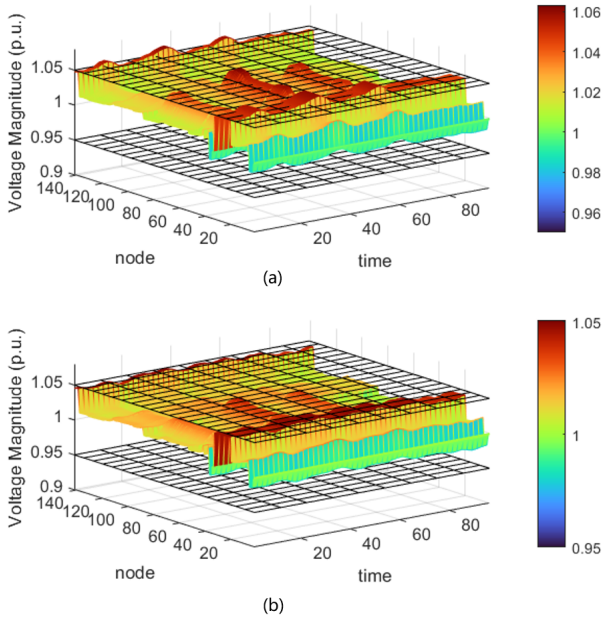

Fig. 12. Comparison of (a) HAPF without load uncertainty and (b) HAPF with load uncertainty in the worst-case scenario.

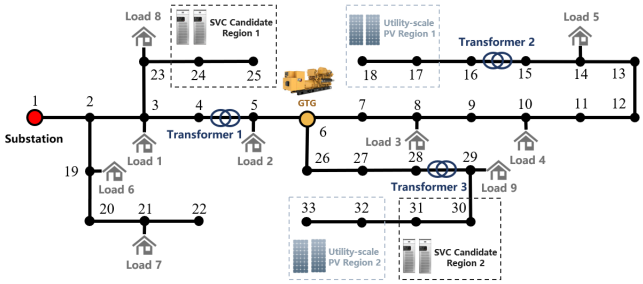

Fig. 13. The modified three-phase 33-bus distribution system.

B. Three-phase 33-bus Test System

The modified three-phase IEEE 33-bus distribution system is shown as Fig. 13. The system includes 9 load buses with the peak being 9.30 MW and 5.76 MVar. The lower and the upper voltage limits are set to 0.95 p.u. and 1.05 p.u., and the apparent power capacity of each branch is 3.5 MVA per phase. Utility-scale PVs are installed at bus 17, 18, 32, 33. We assume that PVs are single-phase integrated, and their power factors can be controlled from -0.95 to 0.95. Two SVCs are installed at two buses out of bus 24, 25, 30, 31, and they are both three-phase devices. Bus 6 is with a three-phase GTG. The voltage ratios of three transformers are set to 1:1.03, 1:1.035 and 1:1.03, respectively.

In this part, we first compare the mismatch of HAPF with linearized adjustable DistFlow model (LAD), and then investigate HC accuracy under unbalanced load levels and structure. Next, we compare the truthfulness of HAPF with stochastic method. Finally, the impact of PV inverter is discussed.

1) Comparison of Mismatch: The accuracy comparison is performed for HAPF and LAD models. In the LAD model, linearized DistFlow [23], [24], [27] is used at both Stage-

TABLE III
MISMATCH COMPARISON OF HAPF TO LAD IN SEVERAL LOAD LEVELS

Rate of Basic Load	Stage	Largest P_{ij} Mismatch (kW)		Largest Q_{ij} Mismatch (kVar)		Largest V_i Mismatch (1×10^{-4} p.u.)	
		HAPF	LAD	HAPF	LAD	HAPF	LAD
100%	1	0.8	40.6	0.7	28.1	2.9	5.7
	2	2.7	46.8	4.8	32.8	2.9	18
95%	1	0.7	39.1	0.6	27.0	3.2	5.5
	2	3.1	44.8	5.5	31.5	3.2	28
90%	1	0.8	35.4	0.7	24.5	2.7	5.1
	2	3.0	42.5	5.3	29.9	2.7	24
85%	1	0.8	32.6	0.7	22.6	2.8	4.9
	2	3.4	39.8	5.9	28.0	2.8	22
80%	1	0.8	33.0	0.6	22.9	2.8	4.8
	2	3.5	38.8	5.8	27.6	2.8	28

[HAPF] hybrid adjustable power flow; [LAD] linearized adjustable DistFlow

1 and -2. Result from the backward/forward is used as a benchmark against that from HAPF and LAD models. At Stage-2, we assume that uncertainty for HAPF and LAD at 12:00 are both equal to 1.90 MW, and then the re-dispatch of controllable resources is attained by $\hat{\boldsymbol{F}}$. The largest power and voltage mismatches under different load levels are illustrated in Table III. It is observed that the largest P_{ij}, Q_{ij} and V_i mismatches are less than 50 kW, 40 kVar and 0.003 p.u., respectively. In the meantime, HAPF outperforms LAD in terms of accuracy by about one order of magnitude in all three columns. For instance, when the rate of basic load is 90 %, the largest P_{ij} mismatch at Stage-2 of HAPF is about 7.1% (i.e., 3/42.5≈7.1%) of that of LAD. That is mainly because HAPF is improved in the loss of power flow, which provides a more accurate linearization and re-dispatch policy.

2) Comparison of HC Accuracy: Due to power and voltage mismatch, HC solved by LAD models may be inaccurate. Besides, the simplified single-phase HAPF model may not be fully applicable for unbalanced systems. Nevertheless, they are both valuable methods because of their simple model complexity compared to three-phase HAPF. To analyze the impacts on HC, the comparison is performed for the three-phase HAPF (3p-HAPF), single-phase HAPF (1p-HAPF) and three-phase LAD (3p-LAD) model. 3p-HAPF is used as a benchmark against other methods. In the 1p-HAPF, the load, SVC and GTG of the three phases are equally divided into one phase.

Firstly, we analyze the impact of unbalanced load on HC inaccuracy in a three-phase system with a balanced structure, where SVCs and GTG are both single-phase integrated and the capacity is the same for each phase. Fig.14 shows the HC solved by 3p-HAPF, 1p-HAPF and 3p-LAD under five unbalanced load levels. "Load Unbalance Degree" represents the ratio of the load of phase-A to the load of phase-C, and the load of phase-B and -A are equal. Fig.14 shows that the HC of 1p-HAPF is almost the same as the 3p-HAPF, while the HC of 3p-LAD is smaller than that of other methods. It indicates that the power and voltage mismatch is a major factor affecting the HC inaccuracy in this case.

Then, we analyze the impact of unbalanced structure on HC inaccuracy in a three-phase system with a balanced load. Two single-phase SVCs are connected to phase-A and one single-phase GTG is connected to phase-C. Fig. 15 shows the HC values with different SVCs. "SVC Cap." means the capacity of each SVC. It shows that the HC of 1p-HAPF is closer to 3p-HAPF than that of 3p-LAD when the SVC capacity is small. For example, when SVC capacity is 0.2 MVar, the HC inaccuracy of 1p-HAPF is only 0.01 MW (i.e., 1.22 - 1.21 = 0.01), while that of 3p-LAD is 0.06 MW (i.e., 1.22 - 1.16 = 0.06). However, the inaccuracy of 1p-HAPF grows with increasing SVC capacity. For instance, when SVC capacity is 0.8 MVar, the HC inaccuracy of 1p-HAPF is 0.1 MW, while that of 3p-LAD is only 0.04 MW.

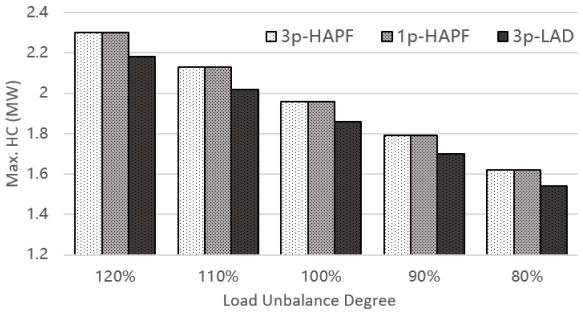

Fig. 14. The HC solved by 3p-HAPF, 1p-HAPF and 3p-LAD in the system with balanced structure but unbalanced load.

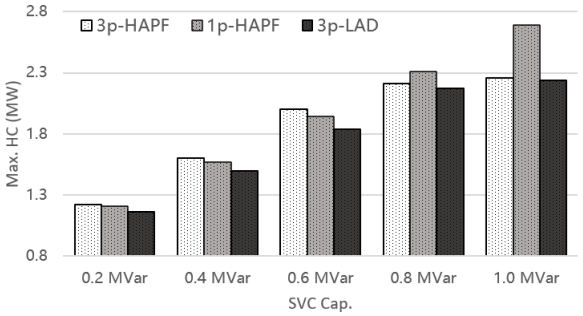

Fig. 15. The HC solved by 3p-HAPF, 1p-HAPF and 3p-LAD in the system with balanced load but unbalanced structure.

In a conclusion, the HC inaccuracy of 1p-HAPF depends on the unbalance degree of system structure, while 3p-LAD is hardly affected by system structure but is limited by power and voltage mismatch. Generally, 1p-HAPF is acceptable to get the HC for the system with a nearly balanced structure. However, 3p-LAD is more applicable than 1p-HAPF for a system with a strongly unbalanced structure.

3) Comparison of Truthfulness: To demonstrate the effectiveness, the two-stage stochastic linearized DistFlow model (SLD) [23], [24] and the proposed model are compared. In the SLD, the first stage decides HC and deployment of SVC before the realization of uncertainty, and the second stage decision variables depend on the uncertain realization. PV and load uncertainties are considered in the two methods, and testing results are shown in Table IV. As a side note, scenarios of SLD are generated by Monte Carlo simulation in this case.

In Table IV, 100 out-of-sample scenarios generated by Monte Carlo simulation are implemented to investigate the truthfulness of HCs attained by these methods. "Occurrence

TABLE IV
COMPARISON OF HAPF WITH SLD

Method	Scenario Num.	HC (MW)	Occurrence Percentage of PV Curtailment (%)
SLD	1	2.74	92
	10	2.24	30
	50	2.14	8
	100	2.08	6
HAPF	Infinite	1.24	0

[HAPF] hybrid adjustable power flow; [SLD] stochastic linearized DistFlow

Percentage of PV Curtailment" represents the percentage of the number of out-of-sample scenarios where PV curtailment occurs. It shows that "HC" solved by SLD under one forecast scenario is as high as 2.74 MW, while PV curtailment occurs in 92% out-of-sample scenarios. The truthfulness of HC increases gradually with the scenario number in SLD. When scenario increases to 100, the HC decreases to 2.08 MW, and PV curtailment occurs in 6% scenarios. It indicates that the "HC" of SLD is over-optimistic and the truthfulness is poor when scenario number is small. In contrast, HAPF method considers all possible scenarios, which are infinite. The HC attained by HAPF is 1.24 MW, and there is no curtailment in out-of-sample scenarios. That is mainly because that HAPF is robust and immune from uncertainty.

4) Impact of Reactive Power: In this subsection, PV inverter is considered as a flexible resource to accommodate uncertainties. The PV inverter can absorb reactive power to lower the voltage level, increasing HC. In the simulation, two single-phase SVCs of 0.2 MVar are connected to phase-A and one three-phase GTG of 1.5 MW is integrated. Fig. 16. depicts three lines to demonstrate the impact of absorbing reactive power. The red dashed line is the voltage level without reactive power control, and the red solid line represents the voltage level with reactive power control, i.e. absorbing reactive by PV inverter. The blue dotted line shows the amount of reactive power at Bus 32.

As shown in the red dashed line, the largest voltage is 1.063 at time 12. By absorbing reactive power, the PV inverter decreases the voltage level to 1.049 at time 12. It indicates that PV inverter can help alleviate overvoltage. The HC increases from 0.92 MW to 1.24 MW, about 74%, by using PV inverter. Therefore, it shows that absorbing reactive power helps increase the HC.

V. CONCLUSION

This paper presents an adjustable model to find the uncertainty-proof hosting capacity (HC). The recourse action in the adjustable model can expand the feasible region of the problem determining HC. We are thus able to increase the uncertainty-proof HC by utilizing the flexible resource in the second stage. Furthermore, the proposed approach provides the closed-form recourse actions when uncertainty occurs. This work proposes a novel hybrid convexification approach to solving the adjustable model. It integrates a successive algorithm and convexification techniques. Simulations are performed with a single-phase 141-node system and a three-phase 33-bus system. The proposed approach shows promising accuracy and robustness.

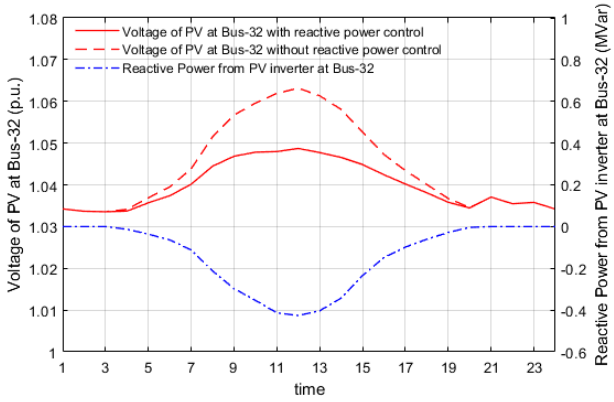

Fig. 16. Voltage magnitude and reactive power of PV at Bus-32 with and without reactive power control in the worst-case scenario.

In future study, we plan to extend the approach to multistage model with storage, and will reduce the model complexity with novel data-driven approaches.

REFERENCES

[1] "Snapshot of global PV markets 2021," International Energy Agency Photovoltaic Power Systems Programme, Tech. Rep., 2021.

[2] A. Samadi, L. Söder, E. Shayesteh, and R. Eriksson, "Static equivalent of distribution grids with high penetration of PV systems," *IEEE Trans. on Smart Grid*, vol. 6, no. 4, pp. 1763–1774, Jul. 2015.

[3] *American National Standard for Electric Power Systems and Equipment-Voltage Ratings (60 Hertz)*, NEMA ANSI Standard C84.1–2011,2011.

[4] S. Wang, Y. Dong, L. Wu, and B. Yan, "Interval overvoltage risk based PV hosting capacity evaluation considering PV and load uncertainties," *IEEE Trans. on Smart Grid*, vol. 11, no. 3, pp. 2709–2721, May 2020.

[5] F. Katiraei and J. R. Agüero, "Solar PV integration challenges," *IEEE Power and Energy Magazine*, vol. 9, no. 3, pp. 62–71, May/Jun. 2011.

[6] R. Torquato, D. Salles, C. O. Pereira, P. C. M. Meira, and W. Freitas, "A comprehensive assessment of PV hosting capacity on low-voltage distribution systems," *IEEE Trans. on Power Delivery*, vol. 33, no. 2, pp. 1002–1012, Apr. 2018.

[7] F. Ding, B. Mather, and P. Gotseff, "Technologies to increase PV hosting capacity in distribution feeders," in *Proc. 2016 IEEE PES General Meeting*, Jul. 2016, pp. 1–5.

[8] "Stochastic analysis to determine feeder hosting capacity for distributed solar PV," Elect. Power Res. Inst., Palo Alto, CA, USA, Tech. Rep. Product ID 1026640, 2012.

[9] D. Bertini, D. Falabretti, M. Merlo, D. Moneta, J. Silva De Assis Carneiro, and A. Silvestri, "Hosting capacity of Italian LV distribution networks," in *Proc. CIRED 2011*, Jun. 2011, pp. 1–4.

[10] O. Babacan, W. Torre, and J. Kleissl, "Siting and sizing of distributed energy storage to mitigate voltage impact by solar PV in distribution systems," *Solar Energy*, vol. 146, pp. 199–208, Apr. 2017.

[11] F. Ding and B. Mather, "On distributed PV hosting capacity estimation, sensitivity study, and improvement," *IEEE Trans. on Sustainable Energy*, vol. 8, no. 3, pp. 1010–1020, Jul. 2016.

[12] P. H. Divshali and L. Söder, "Improving hosting capacity of rooftop PVs by quadratic control of an LV-central BSS," *IEEE Trans. on Smart Grid*, vol. 10, no. 1, pp. 919–927, Jan. 2019.

[13] N. Jayasekara, M. A. Masoum, and P. J. Wolfs, "Optimal operation of distributed energy storage systems to improve distribution network load and generation hosting capability," *IEEE Trans. on Sustainable Energy*, vol. 7, no. 1, pp. 250–261, Jan. 2016.

[14] Z. Hosseini, A. Khodaei, E. Paaso, M. Hossan, and D. Lelic, "Dynamic solar hosting capacity calculations in microgrids," *arXiv preprint arXiv:1809.10133*, 2018.

[15] A. K. Jain, K. Horowitz, F. Ding, K. S. Sedzro, B. Palmintier, B. Mather, and H. Jain, "Dynamic hosting capacity analysis for distributed photovoltaic resources—framework and case study," *Applied Energy*, vol. 280, p. 115633, Dec. 2020.

[16] P. H. Divshali and L. Söder, "Improving PV dynamic hosting capacity using adaptive controller for STATCOMs," *IEEE Trans. on Energy Conversion*, vol. 34, no. 1, pp. 415–425, Mar. 2019.
[17] E. Mulenga, M. H. Bollen, and N. Etherden, "Solar PV stochastic hosting capacity in distribution networks considering aleatory and epistemic uncertainties," *International Journal of Electrical Power & Energy Systems*, vol. 130, p. 106928, Sep. 2021.
[18] S. Stanfield, S. Safdi, S. Mihaly, and S. B. Auck, "Optimizing the Grid-A regulator's guide to hosting capacity analyses for distributed energy resources," Interstate Renewable Energy Council, Tech. Rep., 2017.
[19] Ángel Molina-García, R. A. Mastromauro, T. García-Sánchez, S. Pugliese, M. Liserre, and S. Stasi, "Reactive power flow control for PV inverters voltage support in LV distribution networks," *IEEE Trans. on Smart Grid*, vol. 8, no. 1, pp. 447–456, Jan. 2017.
[20] M. S. S. Abad, J. Ma, D. Zhang, A. S. Ahmadyar, and H. Marzooghi, "Probabilistic assessment of hosting capacity in radial distribution systems," *IEEE Trans. on Sustainable Energy*, vol. 9, no. 4, pp. 1935–1947, Oct. 2018.
[21] C. L. T. Borges, J. F. B. Sousa, and J. Mitra, "PV hosting capacity of LV distribution networks using smart inverters and storage systems: A practical margin," *IET Renewable Power Generation*, vol. 14, no. 8, pp. 1332–1339, Jun. 2020.
[22] A. Ali, K. Mahmoud, and M. Lehtonen, "Maximizing hosting capacity of uncertain photovoltaics by coordinated management of OLTC, VAr sources and stochastic EVs," *International Journal of Electrical Power & Energy Systems*, vol. 127, p. 106627, May 2021.
[23] X. Xu, J. Li, Z. Xu, J. Zhao, and C. S. Lai, "Enhancing photovoltaic hosting capacity—A stochastic approach to optimal planning of static var compensator devices in distribution networks," *Applied Energy*, vol. 238, pp. 952–962, Mar. 2019.
[24] X. Cao, T. Cao, F. Gao, and X. Guan, "Risk-averse storage planning for improving RES hosting capacity under uncertain siting choices," *IEEE Trans. on Sustainable Energy*, vol. 12, no. 4, pp. 1984–1995, Oct. 2021.
[25] X. Chen, W. Wu, and B. Zhang, "Robust capacity assessment of distributed generation in unbalanced distribution networks incorporating ANM techniques," *IEEE Trans. on Sustainable Energy*, vol. 9, no. 2, pp. 651–663, Apr. 2018.
[26] B. Wang, C. Zhang, Z. Dong, and X. Li, "Improving hosting capacity of unbalanced distribution networks via robust allocation of battery energy storage systems," *IEEE Trans. on Power Systems*, vol. 36, no. 3, pp. 2174–2185, May 2021.
[27] S. Wang, S. Chen, L. Ge, and L. Wu, "Distributed generation hosting capacity evaluation for distribution systems considering the robust optimal operation of OLTC and SVC," *IEEE Trans. on Sustainable Energy*, vol. 7, no. 3, pp. 1111–1123, Jul. 2016.
[28] H. Ye, "Surrogate affine approximation based co-optimization of transactive flexibility, uncertainty, and energy," *IEEE Trans. on Power Systems*, vol. 33, no. 4, pp. 4084–4096, Jul. 2018.
[29] G. M. Masters, *Renewable and Efficient Electric Power Systems*. John Wiley & Sons, 2013.
[30] M. Baran and F. Wu, "Optimal sizing of capacitors placed on a radial distribution system," *IEEE Trans. on Power Delivery*, vol. 4, no. 1, pp. 735–743, Jan. 1989.
[31] A. Charnes, W. W. Cooper, and G. H. Symonds, "Cost horizons and certainty equivalents: an approach to stochastic programming of heating oil," *Management science*, vol. 4, no. 3, pp. 235–263, 1958.
[32] R. A. Jabr, "Radial distribution load flow using conic programming," *IEEE Trans. on Power Systems*, vol. 21, no. 3, pp. 1458–1459, Aug. 2006.
[33] S. H. Low, "Convex relaxation of optimal power flow—Part I: Formulations and equivalence," *IEEE Trans. on Control of Network Systems*, vol. 1, no. 1, pp. 15–27, Mar. 2014.
[34] Z. Yang, H. Zhong, A. Bose, T. Zheng, Q. Xia, and C. Kang, "A linearized OPF model with reactive power and voltage magnitude: A pathway to improve the MW-only DC OPF," *IEEE Trans. on Power Systems*, vol. 33, no. 2, pp. 1734–1745, Mar. 2018.
[35] S. F. Santos, D. Z. Fitiwi, M. Shafie-Khah, A. W. Bizuayehu, and J. Catalão, "New multistage and stochastic mathematical model for maximizing RES hosting capacity—Part I: Problem formulation," *IEEE Trans. on Sustainable Energy*, vol. 8, no. 1, pp. 304–319, Jan. 2017.
[36] H. Yuan, F. Li, Y. Wei, and J. Zhu, "Novel linearized power flow and linearized OPF models for active distribution networks with application in distribution LMP," *IEEE Trans. on Smart Grid*, vol. 9, no. 1, pp. 438–448, Jan. 2018.
[37] H. Khodr, F. Olsina, P. De Oliveira-De Jesus, and J. Yusta, "Maximum savings approach for location and sizing of capacitors in distribution systems," *Electric power systems research*, vol. 78, no. 7, pp. 1192–1203, Jul. 2008.
[38] Material of modified three-phase ieee 33-bus distribution system. Aug. 2022. [Online]. Available: https://drive.google.com/drive/folders/1LOHH3DRLqq_A5_iDj4NY_Gg_ya7deVfB?usp=sharing
[39] "Open Power System Data," Oct. 2020. [Online]. Available: https://data.open-power-system-data.org/time_series/2020-10-06

Luomeng Zhang received the B.S. degree in Electrical Engineering from Northwestern Polytechnical University, in 2020. He is currently working towards Ph.D. in Electrical Engineering, Xi'an Jiaotong University. His research interests include renewable integration, and optimal control in power systems.

Hongxing Ye (SM'17) received the B.S. and M.S. degree from Xi'an Jiaotong University (XJTU), Xi'an, China, and the Ph.D. degree from the Illinois Institute of Technology, Chicago, IL, USA, in 2016, all in Electrical Engineering. He is currently a Professor in Dep. of Electrical Engineering, XJTU. He was a tenure-track assistant professor at Cleveland State University, Cleveland, USA, before joining XJTU. His research interests include renewable integration, power system operation, and data-driven optimization in cyber-physical system. He was named outstanding reviewer for IEEE Trans. Sustainable Energy and IEEE Trans. Power Systems.

Fei Ding received her B.S. and M.S. degrees from Tianjin University, China, in 2008 and 2010, respectively, and her Ph.D. degree in Electrical Engineering from Case Western Reserve University, USA in 2014. Now she is a Distinguished Member of Research Staff and Senior Research Engineer at the U.S. National Renewable Energy Laboratory (NREL). Her research interests include renewable energy grid integration, distributed energy resources aggregation and controls, grid resilience and security. She is leading multiple projects at NREL on developing advanced models and controls for managing grid-edge resources to enhance grid flexibility, reliability and resilience, and developing new advanced distribution management system and distributed energy resource management system applications to modernize emerging distribution grids.

Zuyi Li received the B.S. degree from Shanghai Jiaotong University, Shanghai, China, in 1995, the M.S. degree from Tsinghua University, Beijing, China, in 1998, and the Ph.D. degree from the Illinois Institute of Technology (IIT), Chicago, in 2002, all in electrical engineering. Presently, he is a Professor in the Electrical and Computer Engineering Department at IIT. His research interests include economic and secure operation of electric power systems, cyber security in smart grid, renewable energy integration, electric demand management of data centers, and power system protection.

Mohammad Shahidehpour received his Ph.D. degree from the University of Missouri in 1981 in electrical engineering. He is currently the Bodine Chair Professor and Director of the Robert W. Galvin Center for Electricity Innovation at the Illinois Institute of Technology, Chicago. He is the founding Editor-in-Chief of IEEE Transactions on Smart Grid. He is a member of US National Academy of Engineering (NAE).